Colloidal TiO_2 Nanocrystals/MEH-PPV Nanocomposites: Photo(electro)chemical Study

Andrea Petrella,[†] Michela Tamborra,[†] M. Lucia Curri,[‡] Pinalysa Cosma,[†,‡] Marinella Striccoli,[‡] P. Davide Cozzoli,[†] and Angela Agostiano*[,†,‡]

Dipartimento di Chimica, Università di Bari, via Orabona 4, I-70126 Bari, Italy, and CNR IPCF Sezione Bari c/o Dipartimento Chimica, Università di Bari, Via Orabona 4, I-70126 Bari, Italy

Received: July 30, 2004; In Final Form: October 20, 2004

An extensive optical and photoelectrochemical study of blended systems composed of organic-capped TiO_2 nanocrystals with either a spherical or rodlike morphology and a conjugated polymer, MEH-PPV, is presented. The absorption and emission properties of the heterojunctions have been characterized both in solution and in thin films. The blended structures deposited onto conductive substrates have been employed as active layers in photoelectrochemical systems. The investigation has been focused on the photoinduced charge transfer and recombination processes at the interface between the two components, as a function of the nanocrystal shape and surface coating, and of the film thickness. The presence of a large number of interfaces available for charge transfer is believed to play a fundamental role in enhancing the photoelectrochemical performances of the dispersed heterojunctions. The reported results suggest that such MEH-PPV/TiO_2 heterojunctions may be exploited as potential active layers in future photovoltaic and photoelectrochemical devices.

1. Introduction

Composite materials of inorganic semiconductor nanocrystals and conjugated polymers have been the object of great attention in the field of materials for solar energy conversion, due to the possibility of combining the optoelectronic properties of organic polymers with the superior conductivity of inorganic nanoparticles.[1−3] This is because the power conversion efficiency achievable in single-component solar cells remains generally rather poor. For instance, photovoltaic and photoelectrochemical devices based on a polymer as the only active material are intrinsically limited by the extremely low electron mobility through the organic matrix.[1,2] On the other hand, when the active layer is composed of an inorganic semiconductor, the performances suffer for the restricted light fraction that the material can absorb in the visible spectrum.[1]

Recent developments have demonstrated that hybrid inorganic−organic systems offer the potential for enhancing the power conversion efficiency over the level attainable with either component separately.[1,2,4] To this purpose, conjugated polymers and colloidal semiconductor nanocrystals are promising candidates for the low-cost fabrication of large-area photovoltaic devices due both to their peculiar optoelectronic properties and to their processability from solution, which allows facile integration with the existing technologies. These systems are advantageous in that they combine an inorganic material (i.e., the semiconductor nanocrystals), which performs the task of electron transport, with an organic one (i.e., the conjugated polymer), which is able to absorb the solar light as well as to conduct holes.

In particular, conjugated polymers are technologically advantageous owing to the ease of tuning both their energy gaps and their ionization potentials by chemical modification of the polymer chains.[5,6] Nanocrystals are considered more attractive in photovoltaic and photoelectrochemical applications as compared to their bulk counterparts. Nanosized semiconductors show quantum confinement effects that permit tuning of their band gap and modification of the absorption coefficient spectral range by particle size and/or shape modulation.[1,7,8] More importantly, the increase in the surface-to-volume ratio at the nanoscale can be expected to enhance charge carrier percolation across the nanoparticle network, due to extension of the interfacial area available for electron transfer.[1,2,9] In addition, the high electron affinity of semiconductor nanocrystals can match favorably with the low ionization potential of conjugated organic polymers, thus providing a favorable energetics for charge transfer across the heterojunction.

In hybrid organic/inorganic solid-state devices, a mobile charge carrier depletion region is induced at the interface when contacting a p-type organic material with a n-type semiconductor.[10] As the polymer is illuminated by photons of energy higher than the band gap, electron−hole pairs are generated. These excitons diffuse into the organic material and can reach the depletion layer where the internal electric field can induce the separation of the charge carriers.[11] The photogenerated holes can thus migrate along the polymer, while the electrons can move along the nanocrystalline network, ultimately being collected via the respective electrical contacts.[12]

The nature of the charge or energy transfer processes between conjugated polymer and nanocrystals depends on the electrical and optical properties of the two materials, on the surface properties of the nanocrystals, and on the illumination wavelength. The efficiency of these heterojunctions is usually limited by charge recombination phenomena, and the electron transport can also be hindered by surface trap states. These traps can affect the mobility of the charge carriers as well as their recombination probability, in turn resulting in incomplete percolation pathways across the inorganic network.[13] Moreover, in conjugated polymers the diffusion length of excitons is typically about 5−15 nm, so that light excitation occurring far from the interfaces

* Corresponding author. Telephone: +39 0805442060. Fax: +39 0805442129. E-mail: agostiano@area.ba.cnr.it.
† Dipartimento di Chimica.
‡ CNP IPCF Sezione Bari.

10.1021/jp046597c CCC: $30.25
Published on Web 01/08/2005

will decay without any charge transfer from the polymer to the nanocrystals.[14]

To overcome these limitations and to allow for fast charge transfer rates, blending between polymers and nanocrystals has been recently proposed. This strategy provides composite materials having an exciton diffusion length scale similar to that of the blend.[4,15] This condition facilitates the diffusion of the photogenerated exciton to the interface, where it can break up. Interestingly, a rodlike nanocrystal morphology has been recently proven to be more beneficial than a spherical one toward photovoltaic applications owing to the enhancement of directional electron transfer.[15]

Despite the numerous studies that have focused on organic polymer/semiconductor nanocrystal heterojunctions in solid-state devices, the photoelectrochemical investigation of such systems in electrolytic solutions has been scarcely explored so far,[16] except for the case of photoelectrodes consisting of either polymers[17−20] or nanocrystals only.[21−25]

In this work, the extensive photoelectrochemical characterization of thin films composed of either spherical or rodlike surfactant-capped TiO_2 nanocrystals and low-molecular-weight poly[2-methoxy-5-(2′-ethylhexyloxy)-*p*-phenylenevinylene] (MEH-PPV) is presented. TiO_2 is one of the most widely exploited n-type semiconductor in solar energy conversion devices; however, to date it has never been studied as a function of the particle shape and of the nature of the surface organic capping. MEH-PPV is a PPV derivative dispersible in nonpolar solvents and possessing a high degree of structural order, due to the absence of conjugational defects (trans geometry of the double bonds).[26−28] It exhibits a strong bathochromic shift of the main absorption peak with respect to the nonsubstituted PPV due to the electron-donor alkoxy substituents on the polymeric chain.[20] In addition, MEH-PPV is advantageous in that it can be processed more easily than its higher molecular weight counterparts.[29] More importantly, the electron transfer from MEH-PPV to inorganic semiconductors has been demonstrated to be substantially faster than the rate of polymer exciton decay.[10,30]

For the purposes of the present investigation, MEH-PPV was synthesized by the Stille cross-coupling reaction,[26−28] while a colloidal chemistry route has been used to obtain shape-controlled surfactant-capped anatase TiO_2 nanocrystals, highly soluble in nonpolar media.[31]

The prepared TiO_2/MEH-PPV heterojunctions were investigated, both in solution and in films deposited onto low resistivity ITO substrates, by means of steady-state optical spectroscopy and by means of electrochemical measurements. The blend exhibited higher photocurrents than those obtained with the single components, in agreement with the enhancement of MEH-PPV photoexcited electron transfer to TiO_2. In general, the use of spherical TiO_2 nanocrystals provided higher photoelectrochemical responses than their rodlike counterparts.

2. Experimental Section

2.1. Materials. All chemicals were of the highest purity available and were used as received without further purification or distillation. Titanium tetraisopropoxide ($Ti(OPr^i)_4$ or TTIP, 99.999%), trimethylamino-*N*-oxide dihydrate ($(CH_3)_3NO{\cdot}2H_2O$ or TMAO, 98%), water solution), anhydrous ethylene glycol ($HO(CH_2)_2OH$ or EG, 99.8%), oleic acid ($C_{18}H_{33}CO_2H$ or OLEA, 90%), and poly(styrenesulfonate/poly(2,3-dihydrothieno-(3,4-*b*)-1,4-dioxin (PEDOT/PSS) were purchased from Aldrich. Tetrabutylammonium perchlorate ($C_{16}H_{36}ClNO_4$ or TBAP, >99%), lithium perchlorate ($LiClO_4$, >99%), and sodium perchlorate monohydrate ($NaClO_4{\cdot}H_2O$, 98%) were purchased from Fluka. n-Tetradecylphosphonic acid ($C_{14}H_{29}PO(OH)_2$ or TDPA, 98%) was purchased from Alfa Aesar. All solvents used were of analytical grade and purchased from Aldrich. All aqueous solutions were made by using bidistilled water.

SCHEME 1: Molecular Structure of MEH-PPV

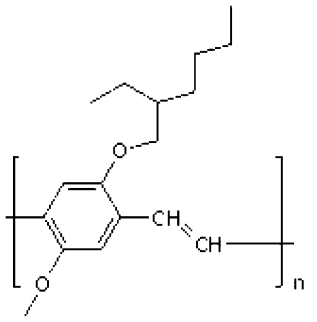

2.2. Procedures. *Synthesis of TiO_2 Nanocrystals.* Organic-capped anatase TiO_2 nanocrystals were synthesized by hydrolysis of titanium tetraisopropoxide (TTIP) using technical oleic acid (OLEA) as surfactant at low temperatures (80−100 °C), as reported elsewhere.[31] Briefly, hydrolysis of TTIP was carried out by an excess of aqueous base solution in the presence of TMAO as catalyst for polycondensation. The morphology of the resulting TiO_2 nanocrystals was modulated by varying the rate of water supply in the reaction mixture. One-dimensional growth was guaranteed by direct injection of large aqueous base volumes into OLEA:TTIP mixtures, while nearly spherical particles were obtained upon the slow in situ release of H_2O resulting from the esterification of OLEA and added EG. The particle size and aspect ratio was changed by varying the TTIP concentration in the growing mixture and/or the reaction time.

After extraction and extensive washing, the OLEA-capped titania nanocrystals resulted in being dispersible in optically clear $CHCl_3$ or hexane solutions. The OLEA capping could be easily replaced by a TDPA capping, as previously described.[31]

Synthesis of MEH-PPV. MEH-PPV (the molecular structure is shown in Scheme 1) has been synthesized by the Stille cross-coupling reaction using (*E*)-1,2-bis(tributylstannyl)ethene and 1,4-diiodo-2,5-di(alkoxy)benzene as the monomers in the presence of Pd catalyst, as previously reported for similar dialkoxy-PPV derivatives.[26−29] Average molecular weights were determined by means of gel permeation chromatographic (GPC) analysis using uniform polystyrene standards and tetrahydrofuran as the solvent. The measured values are $M_n = 2939$ amu and $M_w = 5336$ amu.

Preparation of the Heterojunctions. For the purpose of this work, 0.1 M (expressed in terms of atomic concentrations) $CHCl_3$ solutions of either spherical or rodlike TiO_2 nanocrystals were used. MEH-PPV powder was added to the nanocrystal solutions. The final content of titania in the polymer solution was estimated to be 3.5 wt %. Films with increasing thickness were deposited onto ITO by spin-coating (Chemat Technology spin-coater kw-4b) the prepared solutions at progressively lower speeds (typically 3000−800 rpm).

2.3. Experimental Techniques. Powder X-ray diffraction (XRD) measurements were performed with a D8 Discover-Bruker diffractometer equipped with a 3 kW ceramic tube with a copper anode, a Goebel type parabolic mirror, and a two-bounce monochromator (V Groove) as primary optics, and a NaI(Tl) scintillator detector. A coupled $\theta-2\theta$ movement was chosen for data collection. Concentrated nanocrystal solutions were spread on top of a silicon substrate; then the sample was allowed to dry and measured in reflection geometry.

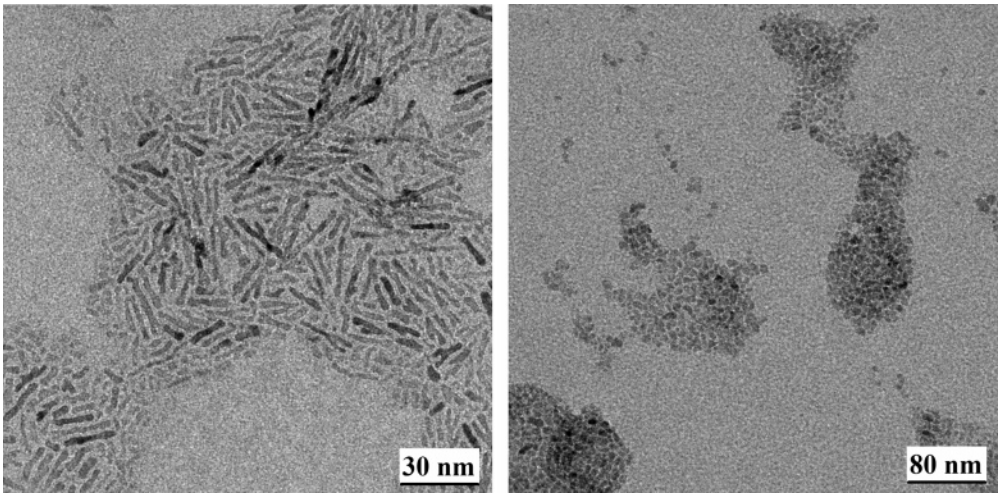

Figure 1. TEM overview of OLEA-capped rodlike (left) and spherical (right) TiO_2 nanocrystals, obtained by TTIP hydrolysis at ~100 °C. The nanorods were prepared using 35 g of OLEA, 5 mmol of TTIP, and 5 mL of 2 M TMAO, with reaction time 24 h. The spherical particles were prepared using 35 g of OLEA, 3.2 g of EG, 1 mmol of TTIP, and 4 mmol of TMAO, with reaction time 48 h.

The morphology and the size of the TiO_2 nanocrystals were checked by transmission electron microscopy (TEM) using a Philips EM 430 microscope operating at 300 kV. The samples for the analysis were prepared by dropping dilute $CHCl_3$ solutions of TiO_2 nanocrystals onto 400-mesh carbon-coated copper grids and leaving the solvent to dry. The samples were stable under the electron beam within the typical observation times.

The film thickness was measured by means of an Alpha-Step 500 surface profiler. Absorption spectra were recorded by using a Cary 3 (Varian) spectrophotometer, while photoluminescence spectra (PL) were measured by using a Cary Eclypse (Varian) fluorescence spectrophotometer. For the PL measurements of thin films, the substrates were arranged at an angle of 45° with respect to the excitation beam.

Photoelectrochemical and electrochemical measurements were carried out with an Autolab potentiostat PGSTAT 10. Chronoamperometric measurements were performed using a classical three-electrode cell (Ag/AgCl reference electrode, ITO working electrode, and platinum counter electrode). The electrolyte solutions were made with either 0.1 M tetrabutylammonium perchlorate (TBAP), lithium perchlorate, or sodium perchlorate in acetonitrile (ACN). The apparatus was equipped with a tungsten lamp (250 W) connected to an optical fiber.

Cyclic voltammetric measurements were carried out in the same cell by employing a glassy carbon as working electrode, an Ag wire as reference electrode, and a platinum counter electrode in a 0.1 M TBAP/ACN solution.

3. Results and Discussion

In this work, spherical TiO_2 nanocrystals with $d \sim 5$ nm (referred to as s-TiO_2) or TiO_2 nanorods of ~3−4 nm in diameter and ~25−30 nm in length (referred to as r-TiO_2) were typically used. Figure 1 reports a low-resolution TEM overview of the as-prepared nanocrystals. The nanoparticles appear spaced on the grid, because of their OLEA surface capping. The titania samples were all in the anatase phase, and the elongation direction of the nanorods was along the *c*-axis, as independently inferred from high-resolution TEM and X-ray diffraction analysis (data not reported), in agreement with the literature.[31]

In Figure 2 the typical UV−vis absorption spectra of MEH-PPV both in chloroform solution and as thin film deposited onto an optically transparent substrate are reported. In the first case,

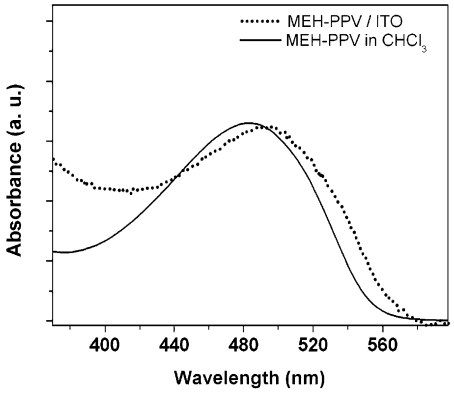

Figure 2. Normalized UV−vis spectra of MEH-PPV in $CHCl_3$ solution (solid line) and as a film deposited onto ITO (dotted line).

TABLE 1: Percentage Decrease of MEH-PPV Luminescence Intensity Measured at λ_{max} (λ_{ex} = 480 nm) as a Function of Film Thickness for MEH-PPV and MEH-PPV/TiO_2 Blends Deposited from a Saturated MEH-PPV Chloroform Solution Containing either 0.1 M Spherical (s-TiO_2) or 0.1 M Rodlike (r-TiO_2) Nanocrystals

	film thickness (nm)	$\lambda_{max,em}$ (nm)	% MEH-PPV PL decrease
MEH-PPV	480 ± 25	603	
MEH-PPV/s-TiO_2 blend	470 ± 30	596	43.5
MEH-PPV/r-TiO_2 blend	465 ± 33	587	52.1
MEH-PPV	196 ± 22	591	
MEH-PPV/s-TiO_2 blend	204 ± 20	595	60.6
MEH-PPV/r-TiO_2 blend	210 ± 22	570	72
MEH-PPV	97 ± 19	590	
MEH-PPV/s-TiO_2 blend	101 ± 16	593	72.9
MEH-PPV/r-TiO_2 blend	98 ± 17	572	88.1

MEH-PPV exhibits a broad band peaked at 480 nm, ascribable to the $\pi \rightarrow \pi^*$ transition of the conjugated polymer. In the polymer film, the $\pi \rightarrow \pi^*$ electronic transition appears broadened and red-shifted. This effect increases with the film thickness, as reported in Table 1.

In Figure 3A, the absorption spectra of MEH-PPV, of rodlike TiO_2 nanocrystals, and of their mixture in $CHCl_3$ are reported. The spectrum of the composite is apparently formed of the two component contributions and no wavelength shift with respect to the pure polymer is observed, thus indicating a negligible

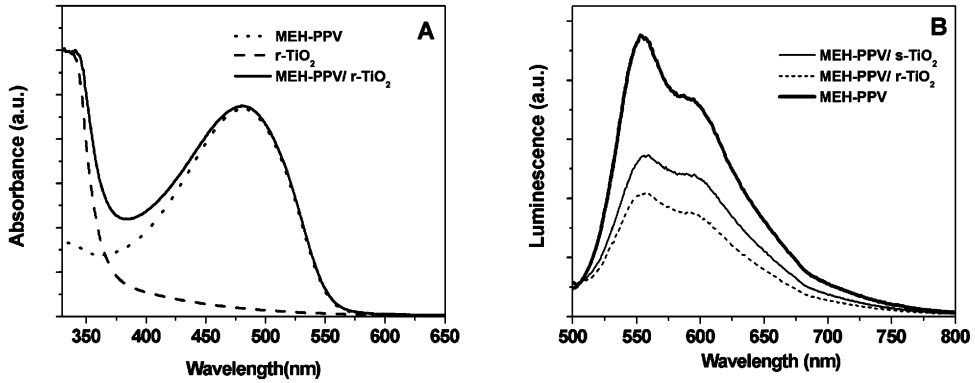

Figure 3. (A) Typical UV−vis spectra of 10^{-4} M MEH-PPV (dotted line), 10^{-3} M organic-capped TiO_2 nanorods (dashed line), and their mixture (solid line) in $CHCl_3$. (B) Photoluminescence spectra of 10^{-4} M MEH-PPV (bold solid line) and its mixture with either 10^{-3} M organic-capped s-TiO_2 (thin solid line) or r-TiO_2 (dotted line) nanocrystal in $CHCl_3$. Excitation was set at $\lambda_{ex} = 480$ nm. OLEA- and TDPA-capped nanocrystals exhibited comparable trends.

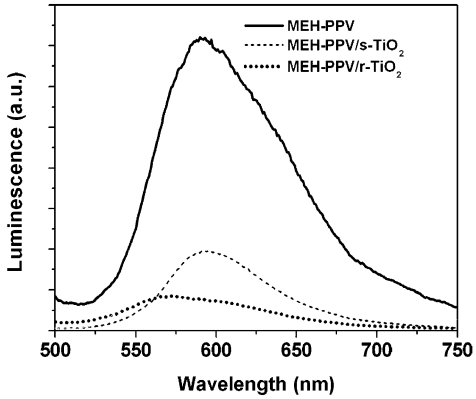

Figure 4. Photoluminescence spectra of films of MEH-PPV (solid bold line) and its blends with s-TiO_2 (dashed line) and r-TiO_2 (dotted line) deposited from a saturated MEH-PPV $CHCl_3$ solution with 0.1 M organic-capped TiO_2 nanocrystals. Films deposited onto ITO. Film thickness was 100 ± 20 nm. Excitation was set at $\lambda_{ex} = 480$ nm. OLEA- and TDPA-capped nanocrystals exhibited comparable trends.

SCHEME 2: Electronic Energy Level Diagram for TiO_2 Nanocrystals and MEH-PPV[a]

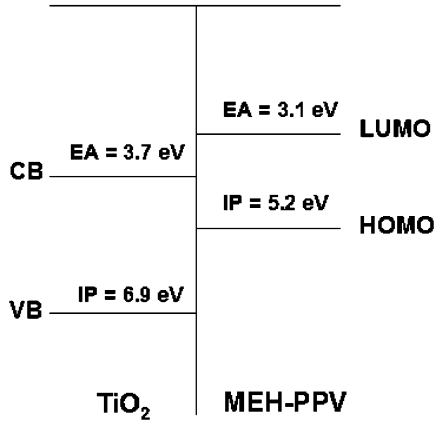

[a] The energy levels were obtained by means of cyclic voltammetry and referred to calomel saturated electrode (IP = ionization potential, EA = electron affinity, CB = conduction band, VB = valence band).

ground-state charge transfer at the heterojunction interfaces.[2] Similar behavior was recorded for blend solutions containing spherical TiO_2 nanocrystals. In Figure 3B the photoluminescence (PL) spectra of pure MEH-PPV and that of its mixture with either spherical or rodlike TiO_2 nanocrystals in solution are shown. The emission features of the polymer are not significantly affected by the presence of the nanocrystals; however, a significant quenching of the emission intensity can be observed. This effect apparently has a dependence on the nanocrystal morphology, being significantly higher in the presence of the TiO_2 nanorods.

Remarkable differences are instead observed for the luminescence spectrum of the polymer deposited film (Figure 4), which appears broader and red-shifted as compared to that in solution. Such PL features can be ascribed to the formation of emissive excimers and/or spatially localized aggregated species, the latter being dependent on the modality of the film preparation.[32] The simultaneous analysis of the absorption and PL data reported in Figures 2−4 can also support the possibility that, upon polymer deposition, J-aggregates can be formed with transition dipoles parallel to the molecular plane.[33,34]

When a mixture of MEH-PPV and TiO_2 spherical nanoparticles is spin-coated onto ITO, a relevant quenching of the polymer emission is observed, which appears more accentuated in the case of the blend with r-TiO_2. In the PL spectrum of the MEH-PPV/r-TiO_2 heterojunction, a significant blue shift of the polymer emission is also detected. Table 1 reports the behavior of the PL intensity and the shift values in the position of the PL band for polymer films at different thicknesses and containing TiO_2 nanocrystals of different shapes. Films were prepared by spin-coating mixtures of the polymer and different weight percentages of OLEA molecules (up to 3.5%), the capping agents for the nanoparticles. In no case were the luminescence spectra significantly different from those recorded for the polymer alone. This allowed exclusion of a direct involvement of OLEA in the quenching processes or the onset of effects related to the change in the refractive index due to presence of a different material.

The fluorescence quenching in the presence of TiO_2 nanocrystals can be attributed to either energy or charge transfer from the polymer to the inorganic semiconductor. Although a Förster energy transfer mechanism has been recently invoked for CdSe, InP, and PbS nanocrystals embedded in MEH-PPV,[35,36] it can be excluded in our case, due to the lack of overlap between TiO_2 absorption and MEH-PPV emission spectrum. On the basis of the relative positions of MEH-PPV and TiO_2 energy levels, the dissociation of the exciton at the interface between the two materials is energetically allowed (Scheme 2).[1]

Consequently, the transfer of MEH-PPV photogenerated electrons to TiO_2 conduction band should be responsible for the polymer emission quenching in Figures 3 and 4. The presence of an organic capping on the nanocrystal surface has been reported to form a barrier that prevents charge transfer at

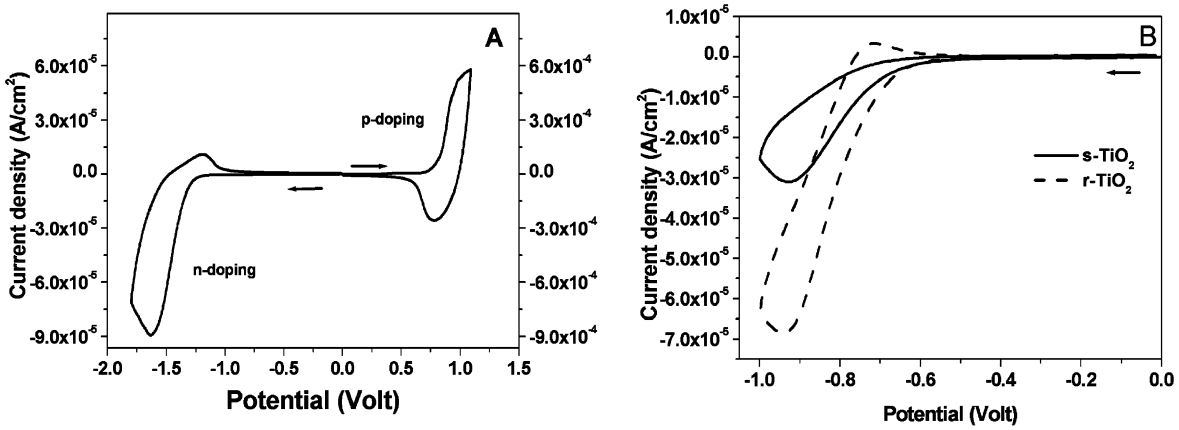

Figure 5. (A) Cyclic voltammetry of MEH-PPV in 0.1 M TBAP/ACN. (B) Cyclic voltammetry reduction cycle of OLEA-capped r-TiO_2 (dashed line) and OLEA-capped s-TiO_2 (solid line) in 0.1 M TBAP/ACN.

the interface with the polymer.[2] In such a case, no quenching of the fluorescence was observed and either chemical[37] or thermal[38] treatments of the nanocrystal surface were, in fact, required to allow the charge transfer upon ligand removal. In contrast, in our system the charge separation and transfer processes took place at the interface with the MEH-PPV, irrespective of the presence of the organic capping on the TiO_2 surface, although an energy transfer process was ruled out to account for the MEH-PPV emission properties. Our findings are supported by a recently published LESR (light-induced electron spin resonance) study that highlights the strict dependence of electron transfer between nanocrystals and conjugated polymers on the nature of the surface coating.[36]

Because in rodlike nanocrystals the surface-to-volume ratio is higher than in spheres, the increase of polymer emission quenching can be correlated with a higher probability of charge transfer at the MEH-PPV/TiO_2 interface. In addition, with rod-shaped particles the number of nanocrystal−nanocrystal hops required for charge transport can be reduced, hence enhancing the probability for electrons to find a pathway to escape recombination with holes.[15,38]

As a general trend, as the blend film is made progressively thicker (see Table 1), the MEH-PPV luminescence quenching reduces and a shift of the emission maximum to longer wavelengths is observed. Even at the low nanocrystal content used in the present system, the possible formation of nanocrystal aggregates may be envisaged, as similarly found in the case of CdSe/MEH-PPV nanocomposite films.[2] The presence of only a few fractions of nanocrystals in physical contact with several others is also confirmed by Salafsky[1], who assumed the polymer to be continuous throughout the composite. Thus, the observed red shift can be more likely related to an increase in the polymer aggregation in thicker films that would result in a lower number of interfaces with the nanocrystals, in turn leading to a less efficient charge transfer process and a less dramatic MEH-PPV emission quenching. Accordingly, the blue shift in the PL spectrum of MEH-PPV/r-TiO_2 can be possibly ascribed to the hindering of polymer aggregation, somehow depending on the modality through which the polymer molecules may intercalate through the hydrocarbon moieties of the surfactants on the TiO_2 surface. Alternatively, the possibility that it can originate from nonequilibrated excited states cannot be excluded.

Figure 5A reports the cyclic voltammetric behavior of an MEH-PPV film deposited by casting onto a glassy carbon substrate. The presence of $(Bu)_4N^+$ ion served to protect the polymer from any damage to the conjugation, keeping its electroactivity stable in time.[18] The reduction of MEH-PPV shows a quasi-reversible electrochemical doping/dedoping process, while the polymer oxidation (p-doping) is characterized by a quasi-reversible electrochemical response with a charge transport mechanism controlled by the diffusion of the counterions in the film.[18]

TABLE 2: Electrochemical Evaluation of MEH-PPV Energy Gap (E_g) from the Voltammogram in Figure 5A[a,b]

		energetic levels (eV)		
ϕ_p (V vs Ag)	ϕ_n (V vs Ag)	HOMO	LUMO	E_g (eV)
+0.+0.84	−1.27	−5.24	−3.13	2.11

[a] The accuracy of E_g ($=e\Delta\phi$) is ±0.08 eV. [b] The onset potentials, ϕ_n and ϕ_p, were determined from the intersection of the tangent drawn at the rising reduction and oxidation curves, respectively, with the correspondening background current.

The energy gap of the polymer ($E_g = e\Delta\phi$) can be calculated from the difference between the energies of the LUMO and HOMO levels, which can be evaluated (Table 2) from the onset potential of the n-doping (ϕ_n) and p-doping (ϕ_p) processes, respectively. The energy levels can be estimated with respect to SCE (saturated calomel electrode) as the reference electrode by adding 4.4 eV to the corresponding measured electrochemical potentials.[17] Thus, $E_{LUMO} = -e(\phi_n + 4.4)$ and $E_{HOMO} = -e(\phi_p + 4.4)$. The obtained energy gap value ($E_g = e\Delta\phi$) is quite close to that extrapolated from the absorption onset, i.e., the optical energy gap (2.17 eV), which demonstrates the reliability of the electrochemical evaluation of the LUMO and HOMO energy levels.

In Figure 5B, the cathodic current/potential behaviors of both s-TiO_2 and r-TiO_2 nanocrystalline electrodes are compared. As nanocrystalline electrodes are characterized by a high surface-to-volume ratio, their electrochemical properties can be expected to be strongly influenced by surface defects or adsorbed species.[39] In addition, the pores between the nanoparticles are filled with electrolyte, so electron transport is driven by a concentration gradient rather than by electric fields. The reported cyclic voltammogram evidences the processes of electron accumulation and following discharge in the film, which are superimposed on a faradaic current, probably due to oxygen trapped in the electrolyte. The cathodic peak appearing at around −1 V can be also attributed to the reduction of surface Ti(IV) according to Koelsch et al.[24] The increased value of the current relative to TiO_2 nanorods is consistent with an easier charge transfer process as compared to the spherical TiO_2 nanocrystals.

In Figure 6 the n- and p-doping processes for MEH-PPV/TiO_2 nanocrystals blended films are reported. In the reduction cycle (Figure 6A), the MEH-PPV blend with s-TiO_2 exhibits

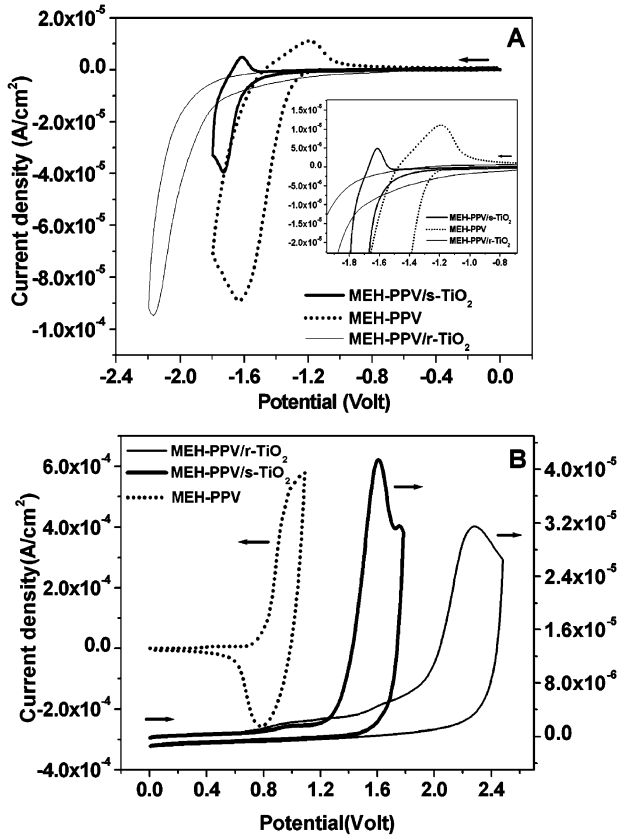

Figure 6. Cyclic voltammetry reduction (A) and oxidation cycle (B) of MEH-PPV (dotted line), MEH-PPV/OLEA-capped r-TiO_2 (thin solid line), and MEH-PPV/OLEA-capped s-TiO_2 (bold solid line) in 0.1 M TBAP/ACN. MEH-PPV/r-TiO_2 and MEH-PPV/s-TiO_2 are referred to the right axis of current; MEH-PPV is referred to the left axis of current. Inset: enlargement of the region around 0 V.

TABLE 3: Electrochemical Evaluation of ϕ_n, ϕ_p, HOMO Energies, and LUMO Energies for Films of MEH-PPV, s-TiO_2, r-TiO_2, and MEH-PPV/TiO_2 Blends, as Estimated from Data in Figures 5 and 6[a]

	ϕ_p (V vs Ag)	ϕ_n (V vs Ag)	E_{HOMO} (eV)	E_{LUMO} (eV)
MEH-PPV	+0.84	−1.27	−5.24	−3.13
MEH-PPV/s-TiO_2	+1.34	−1.59	−5.74	−2.81
MEH-PPV/r-TiO_2	+2.02	−1.82	−6.42	−2.58
s-TiO_2		−0.71		−3.69
r-TiO_2		−0.72		−3.67

[a] The accuracy for the HOMO and LUMO energies is ±0.08 eV.

n-doping and n-dedoping peaks shifted to higher potentials with respect to those found for the bare polymer. By contrast, the MEH-PPV blend with r-TiO_2 is characterized by an irreversible n-doping process, being further shifted toward negative potentials. In the oxidation cycle (Figure 6B), for both blends, only an irreversible p-doping is observed, appearing shifted to higher potentials as compared with that for the polymer alone. In particular, the shift for the TiO_2 nanorod-containing film is higher than the one observed with the spherical TiO_2 nanoparticles. In this case, the blends show current intensities of 1 order of magnitude lower than that for MEH-PPV, as opposed to what is observed in reduction (see Table 3). The shift to higher potentials of both the n- and p-doping curves suggests a lower ionic conductivity and/or a slower ionic motion in the blended films with respect to that in the bare polymer. The lower oxidation current can be attributed either to some dissolution of the oxidized form of the film, following the shift toward more positive potentials,[40] or to a decrease in the p-conductivity of the polymer by the presence of the inorganic semiconductor. The irreversibility of the p-doping processes can arise from overoxidation of the polymer, caused by the high operating voltage, which can result in its complete electroinactivation.[18]

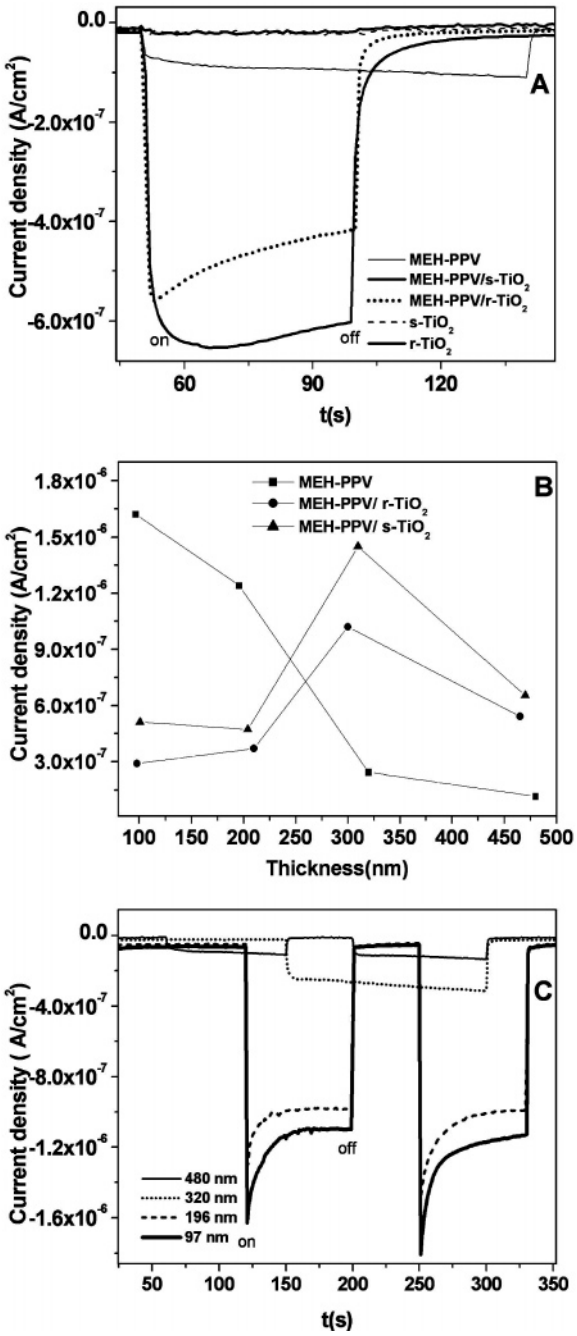

Figure 7. (A) Chronoamperometric measurements (at 0 V bias) of films of MEH-PPV (thin solid line), r-TiO_2 (gray line), s-TiO_2 (dashed line), MEH-PPV/s-TiO_2 blend (bold solid line), and MEH-PPV/r-TiO_2 blend (dotted line) in a photoelectrochemical cell. The films (450 ± 30 nm) were deposited onto ITO. (B) Chronoamperometric measurements (at 0 V bias) of films of MEH-PPV, MEH-PPV/s-TiO_2 blend, and MEH-PPV/r-TiO_2 blend with different thickness. (C) Chronoamperometric measurements (at 0 V bias) of MEH-PPV films with different thickness. The TiO_2 nanoparticles were capped with OLEA.

In Figure 7A, the photoresponses of ITO electrodes (at 0 V bias) covered with MEH-PPV, TiO_2 nanocrystals, and MEH-PPV/TiO_2 blends are reported. It is apparent that a significant increase of the photocurrents results from the combination of the two components.[4] Moreover, the photocurrents are very reproducible, as opposed to the signals obtained with the bare

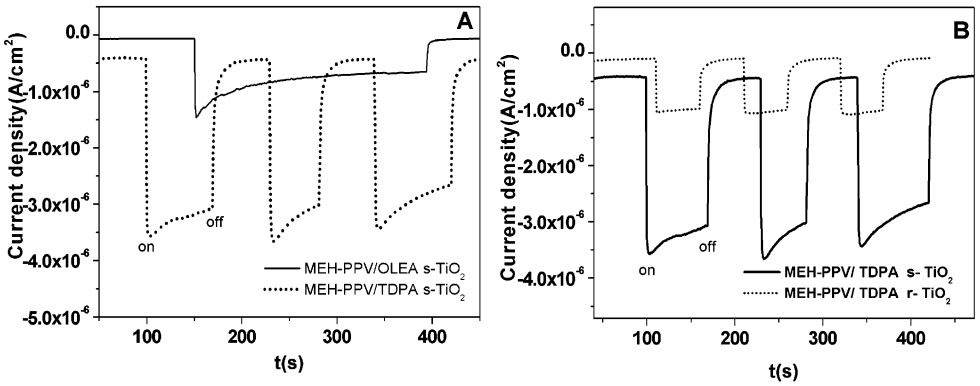

Figure 8. (A) Chronoamperometric measurements (at 0 V bias) of films of MEH-PPV/OLEA-capped s-TiO_2 (solid line) and MEH-PPV/TDPA-capped s-TiO_2 (dotted line). (B) Chronoamperometric measurements (at 0 V bias) of films of MEH-PPV/TDPA-capped s-TiO_2 (solid line) and MEH-PPV/TDPA-capped r-TiO_2 (dotted line) blends in a photoelectrochemical cell. The films (300 ± 20 nm) were deposited onto ITO and immersed into a 0.1 M TBAP/ACN solution.

TiO_2 nanocrystals. The analysis of the light-generated currents in a photoelectrochemical cell is always a complex problem, due to the concurring contributions of charge transport inside the film and charge injection toward the electrodes and/or the electrolyte solution. Consequently, both the morphology of the film and the nature of the surface in contact with the solution should play a relevant role. In our case, we can assume that a large number of interfaces at the organic/inorganic hybrid structure can allow the photogenerated electrons to be readily transferred from MEH-PPV to the TiO_2 conduction band, thus successfully competing with the deactivation processes inside the polymer. In the composite systems, while the polymer phase is usually continuous throughout the film, only a fraction of the nanocrystals is supposed to be characterized by particles in extensive physical contact with each other. As comparatively fewer percolation pathways are available for the electrons through the nanocrystalline phase when compared to those useful for the holes through the polymer matrix, the photocurrents can be therefore expected to be limited by electron transport rather than by hole transport.[1] In this regard, the morphology and the surface state of the oxide nanoparticles may play a relevant role in affecting the overall electron transport within the blends. On the basis of the above-described phenomena, the cathodic nature of the photocurrents can be reasonably ascribed to electron injection to the electrolyte solution rather than to the electrode.

The effect of the film thickness on the photocurrent intensity is reported in Figure 7B. The photocurrent of bare MEH-PPV (Figure 7C) decreases with increasing film thickness, as expected from the enhanced probability of electron−hole recombination when the photoexcited charge carriers have to move through longer percolation pathways.[41] Moreover, for thinner MEH-PPV films, the photocurrents exhibited an initial exponential behavior, which is typical for a charging/discharging process,[17] originating from electron injection into the polymer LUMO, followed by hole recombination.

For the blends (Figure 7B), the photocurrents of films increase in the thickness range of 450−300 nm, owing to the previously discussed influence of polymer aggregation (Table 1). As the blend thickness further decreases below 300 nm, the photoactivity tends to be reduced, whereas a contemporary reduction of the PL signal is observed. This discrepancy may indicate that, in thinner films, the efficiency is more likely affected by charge transfer to the electrolyte that permeates the porous blend.

From the data in Figure 7, blends containing spherical TiO_2 particles showed higher photoactivity compared to rods. This represents a surprising result. A rodlike geometry is, in fact, expected to be favorable toward a more efficient packing of the inorganic units, being driven by the higher contact area and the more intensive van der Waals forces than in spheres, which should ultimately enhance the photoconversion process.[15] While the increase in the emission quenching observed in Figure 4 demonstrates a higher probability of charge transfer for TiO_2 nanorods at the MEH-PPV/TiO_2 interfaces, the photoelectrochemical measurements suggests the existence of a limited number of charge separation pathways, probably related to a disordered orientation of the inorganic transporters in the films.[42]

As shown in Figure 8A, the presence of a different surfactant, such as TDPA, on the titania surface leads to improved photoactivity with respect to the OLEA capping.[43] It is known[44] that the anchoring of phosphonic acids to the titanium oxide surface can involve both the condensation of P−OH groups with surface titanol groups and the coordination of the phosphoryl oxygen to Lewis acid sites in a tridentate bonding mode that is more stable with respect to the bidentate bonding mode adopted by carboxylic ligands. When compared to OLEA, TDPA can also offer a lower energetic barrier against interparticle electron transport due to its reduced sterical hindrance, thus explaining the enhanced photoconversion process. Also, TDPA-coated spherical particles present higher photocurrents with respect to the case of rods (Figure 8B). These data further confirm the assumption that the processes of charge transfer in our system can take place even without any specific treatment of the interfaces between the organic-capped oxide nanocrystals and the polymer.

The effect of electrolyte counterion charge and dimensions on film photoactivity has been also studied, and the results are reported in Figure 9. In the case of the bare MEH-PPV (Figure 9A), comparatively stronger photocurrents are recorded if Li^+ is used in place of $(Bu)_4N^+$ or Na^+ counterions. This experimental result contradicts the previously reported Li^+-induced inactivation of the polymer n-doping processes.[18] Because of its smaller size, Li^+ can easily penetrate the film interstices, thus neutralizing negative charges and consequently enhancing hole release. $(Bu)_4N^+$ and Na^+ are larger ions carrying a lower charge density, so a lower ionic conductivity can be established through the polymer. Moreover, in the presence of Na^+, an easy diffusion along the film can be hindered, being confirmed by the complete absence of capacitive behavior. However, in the case of heterojunctions (Figure 9B), a modest enhancement of the photoactivity is obtained with s-TiO_2 in the presence of Na^+, whereas in composites with r-TiO_2, the highest photoresponse (Figure 9C) is again recorded in Li^+ salt solution.

If a layer of PEDOT/PSS is interposed between the ITO contact and the blend film, a slight improvement of the

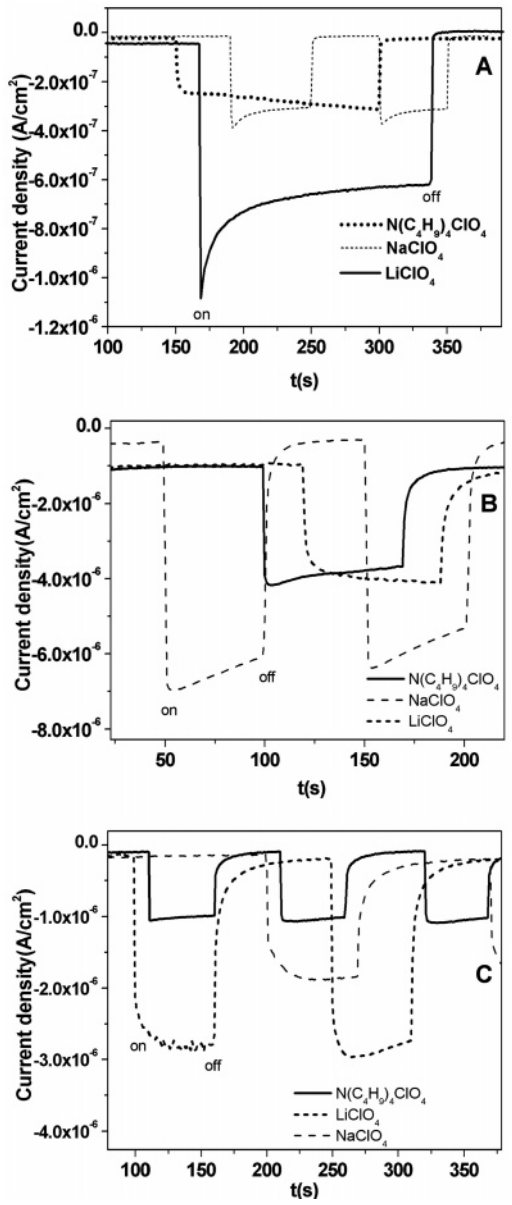

Figure 9. (A) Chronoamperometric measurements (at 0 V bias) of films of MEH-PPV immersed into a 0.1 M TBAP (bold dotted line), 0.1 M sodium perchlorate (dotted line), and 0.1 M lithium perchlorate (solid line) ACN solution in a photoelectrochemical cell. (B) Chronoamperometric measurements (at 0 V bias) of films of MEH-PPV/s-TiO_2 in a 0.1 M TBAP (solid line), sodium perchlorate (dashed line), and lithium perchlorate (short dashed line) ACN solution in a photoelectrochemical cell. (C) Chronoamperometric measurements (at 0 V bias) of films of MEH-PPV/r-TiO_2 immersed into a 0.1 M TBAP (solid line), 0.1 M sodium perchlorate (dashed line), and 0.1 M lithium perchlorate (short dashed line) ACN solution in a photoelectrochemical cell. Nanocrystalline TiO_2 particles were TDPA capped. The films (300 $\pm$ 20 nm) were deposited onto ITO.

photoconversion process is observed. Figure 10 reports the representative case of an MEH-PPV/TDPA-capped s-TiO_2 heterojunction. The presence of PEDOT/PSS has been reported to influence the charge transfer process.[15] Because of its high proton conductivity, it can effectively contribute to a more efficient photoelectrochemical conversion.[45] In Figure 11 the photocurrents obtained for blends with a varying nanocrystal content are compared. Interestingly, by decreasing the TiO_2 concentration in the mixture by a factor of 10, a significant increase of the photocurrent is obtained, although the photoluminescence spectra of the films show a more effective MEH-

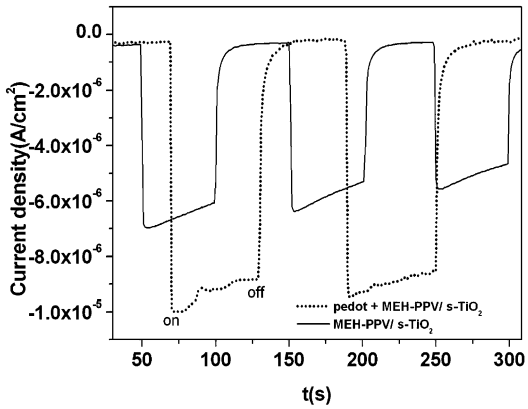

Figure 10. Chronoamperometric measurements (at 0 V bias) of films of PEDOT/PSS/MEH-PPV/TDPA-capped s-TiO_2 (dotted line) and MEH-PPV/TDPA-capped s-TiO_2 (solid line). The films were deposited onto ITO and immersed into a 0.1 M $NaClO_4$/ACN solution.

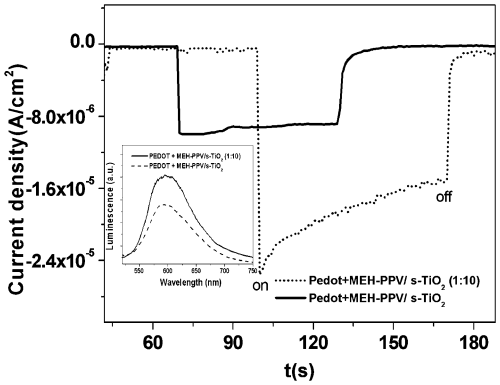

Figure 11. Chronoamperometric measurements (at 0 V bias) of films of PEDOT/PSS/MEH-PPV/TDPA-capped s-TiO_2 (0.1 M in the starting solution) and PEDOT/PSS/MEH-PPV/TDPA-capped s-TiO_2 (0.01 M in the starting solution). The films were deposited onto ITO and immersed into a 0.1 M $NaClO_4$/ACN solution. Inset: photoluminescence spectra of both films. Excitation was set at $\lambda_{ex} = 480$ nm.

PPV PL quenching in the presence of higher concentration of nanocrystals.[1] A lower concentration of TiO_2 may result in a reduction of nanocrystal phase segregation, thus increasing the charge transfer processes between the components of the mixture in the photoelectrochemical device.

4. Conclusions

The photoinduced charge transfer and recombination processes in MEH-PPV−TiO_2 nanocrystal blended structures have been studied as a function of the shape of the titania nanocrystals and of their surface organic coating.

The charge separation and transfer processes have been proven to occur at the interface with MEH-PPV, irrespective of the presence of the organic capping on the TiO_2 surface. The composite films apparently showed a higher photoactivity when compared to the single components due to the availability of numerous interfaces for enhanced charge transfer at the heterojunction. The use of spherical TiO_2 nanocrystals provided higher photoelectrochemical responses than their rodlike counterparts. Blend films containing phosphonic acid capped TiO_2 nanocrystals exhibited higher photocurrents with respect to the hybrids containing titania capped with the bulkier oleic acid molecules. The reported results suggest that such organic−inorganic heterojunctions may be exploited as potential active layers in photovoltaic and photoelectrochemical devices.

Acknowledgment. The authors wish to thank Prof. Francesco Naso, Prof. Francesco Babubri, and Prof. Gianluca Maria Farinola for providing MEH-PPV samples and for many helpful discussions.

References and Notes

(1) Salafsky, J. S. *Phys. Rev. B* **1999**, *59*, 10885.
(2) Greenham, N. C.; Peng, X.; Alivisatos, A. P. *Phys. Rev. B* **1996**, *54*, 17628.
(3) Sun, B.; Marx, E.; Greenham, N. C. *Nano Lett.* **2003**, *3*, 961.
(4) Nelson, J. *Curr. Opin. Solid State Mater. Sci.* **2002**, *6*, 87.
(5) Grem, G.; Leditzky, G.; Ullrich, B.; Leising, G. *Adv. Mater.* **1992**, *4*, 36.
(6) Greenham, N. C.; Moratti, S. C.; Bradley, D. D. C.; Friend, R. H.; Holmes, A. B. *Nature* **1993**, *365*, 628.
(7) Alivisatos, A. P. *J. Phys. Chem.* **1996**, *100*, 13226.
(8) Alivisatos, A. P. *Science* **1996**, *271*, 933.
(9) Huynh, W. U.; Dittmer, J. J.; Teclemariam, N.; Milliron, D. J.; Alivisatos, A. P. *Phys. Rev. B* **2003**, *67*, 115326.
(10) Savenije, T.; Warman, J. M.; Goossens, A. *Chem. Phys. Lett.* **1998**, *287*, 148.
(11) Ginger, D. S.; Greenham, N. C. *Synth. Met.* **2001**, *124*, 117.
(12) Nozik, A. *J. Phys.* **2002**, *E14*, 115.
(13) Dittmer, J. J.; Marseglia, E. A.; Friend, R. H. *Adv. Mater.* **2000**, *12*, 1270.
(14) Anderson, N. A.; Hao, E.; Ai, X.; Hastings, G.; Lian, T. *Chem. Phys. Lett.* **2001**, *347*, 304.
(15) Huynh, W. U.; Dittmer, J.; Alivisatos, A. P. *Science* **2002**, *295*, 2425.
(16) Petrella, A.; Tamborra, M.; Cozzoli, P. D.; Curri, M. L.; Striccoli, M.; Cosma, P.; Farinola, G. M.; Babudri, F.; Naso, F.; Agostano, A. *Thin Solid Films* **2004**, *451*, 64.
(17) Li, Y.; Cao, Y.; Gao, J.; Wang, D.; Yu, G.; Heeger, A. J. *Synth. Met.* **1999**, *99*, 243.
(18) Yang, C.; He, G.; Wang, R.; Li, Y. *J. Electroanal. Chem.* **1999**, *471*, 32.
(19) Yang, C.; Zheng, J.; Fan, L.; Li, Y. *Supramol. Sci.* **1998**, *5*, 519.
(20) Ram, M. K.; Sarkar, N.; Bertoncello, P.; Sarkar, A.; Narizzano, R.; Nicolini, C. *Synth. Met.* **2001**, *122*, 369.
(21) Tsujiko, A.; Itoh, H.; Kisumi, T.; Shiga, A.; Murakoshi, K.; Nakano, Y. *J. Phys. Chem. B* **2002**, *106*, 5878.
(22) Shiga, A.; Tsujiko, A.; Ide, T.; Yae, S.; Nakano, Y. *J. Phys. Chem. B* **1998**, *102*, 6049.
(23) Oliva, F. Y.; Avalle, L. B.; Santos, E.; Camara, O. R. *J. Photochem. Photobiol., A: Chem.* **2002**, *146*, 175.
(24) Koelsch, K.; Cassaignon, S.; Guillemoles, J. F.; Jolivet, J. P. *Thin Solid Films* **2002**, *404*, 312.
(25) de Jong, P. E.; Vanmaekelbergh, D. *J. Phys. Chem. B* **1997**, *101*, 2716.
(26) Babudri, F.; Cardone, A.; Chiavarone, L.; Ciccarella, G.; Farinola, G. M.; Naso, F.; Scamarcio, G. *Chem. Commun.* **2001**, 1940.
(27) Babudri, F.; Cicco, S. R.; Farinola, G. M.; Naso, F.; Bolognesi, A.; Porzio, W. *Macromol. Rapid Commun.* **1996**, *17*, 905.
(28) Naso, F.; Babudri, F.; Farinola, G. M. *Pure Appl. Chem.* **1999**, *71*, 1485.
(29) Babudri, F.; Cicco, S. R.; Chiavarone, L.; Farinola, G. M.; Lopez, L. C.; Naso, F.; Scamarcio, G. *J. Mater. Chem.* **2000**, *10*, 1573.
(30) Van Hal, P. A.; Christiaans, M. P. T.; Wienk, M. M.; Kroon, J. M.; Janssen, R. A. J. *J. Phys. Chem. B* **1999**, *103*, 4352.
(31) Cozzoli, P. D.; Kornowski, A.; Weller, H. *J. Am. Chem. Soc.* **2003**, *125*, 14539.
(32) Nguyen, T. Q.; Martini, I. B.; Liu, J.; Schwartz, B. *J. Phys. Chem.* **2000**, *104*, 237.
(33) Liu, Y.; Li, Q.; Xu, Y.; Jiang, X.; Zhu, D. *Synth. Met.* **1997**, *85*, 1279.
(34) Kalyasundaram, K.; Gratzel, M. *Coord. Chem. Rev.* **1998**, *177*, 347.
(35) Chang, T.-W. F.; Musikhin, S.; Bakueva, L.; Levina, L.; Hines, M. A.; Cyr, P. W.; Sargent, E. H. *Appl. Phys. Lett.* **2004**, *84* (21), 4295.
(36) Pientka, M.; Dyakonov, V.; Meissner, D.; Rogach, A.; Talapin, D.; Weller, H.; Lutsen, L.; Vanderzande, D. *Nanotechnology* **2004**, *15*, 163.
(37) Greenham, N. C.; Peng, X.; Alivisatos, A. P. *Synth. Met.* **1997**, *84*, 545.
(38) Huynh, W. U.; Dittmer, J. J.; Libby, W. C.; Whiting, G. L.; Alivisatos, A. P. *Adv. Funct. Mater.* **2003**, *13*, 73.
(39) Willis, R. L.; Olson, C.; O'Regan, B.; Lutz, T.; Nelson, J.; Durrant, J. R. *J. Phys. Chem. B* **2002**, *106*, 7605.
(40) Richter, M. M.; Fan, F. F.; Klavetter, F.; Heeger, A. J.; Bard, A. J. *Chem. Phys. Lett.* **1994**, *226*, 115.
(41) Hagfeldt, A.; Gratzel, M. *Chem. Rev.* **1995**, *95*, 49.
(42) Bakueva, L.; Musikkin, S.; Hines, M. A.; Chang, T. W. F.; Tzolov, M.; Scholes, G. D.; Sargent, E. H. *Appl. Phys. Lett.* **2003**, *82*, 2895.
(43) Kim, Y. G.; Walker, J.; Samuelson, L. A.; Kumar, J. *Nano Lett.* **2003**, *3*, 523.
(44) Guerrero, G.; Mutin, P. H.; Vioux, A. *Chem. Mater.* **2001**, *13*, 4367.
(45) Lefebre, M.; Qi, Z.; Rana, D.; Pickup, P. G. *Chem. Mater.* **1999**, *11*, 262.